

Nonlinear equation for curved nonstationary flames and flame stability

V. V. Bychkov

Department of Plasma Physics, Umea University, S-901 87 Umea, Sweden

K. A. Kovalev

*Department of Physics, Uppsala University, Box 530, S-751 21 Uppsala, Sweden
and Moscow Institute of Physics and Technology, 141 700 Dolgoprudny, Moscow Region, Russia*

M. A. Liberman

*Department of Physics, Uppsala University, Box 530, S-751 21 Uppsala, Sweden
and P. Kapitsa Institute for Physical Problems, 117 334 Moscow, Russia*

(Received 16 February 1999)

A time-dependent nonlinear equation for a nonstationary curved flame front of an arbitrary expansion coefficient is derived under the assumptions of a small but finite flame thickness and weak nonlinearity. On the basis of the derived equation, stability of two-dimensional curved stationary flames propagating in tubes with ideally adiabatic and slip walls is studied. The stability analysis shows that curved stationary flames become unstable for sufficiently wide tubes. The obtained stability limits are in a good agreement with the results of numerical simulations of flame dynamics and with semiquantitative stability analysis of curved stationary flames. Possible outcomes of the obtained instability at the nonlinear stage are discussed. The instability may result in extra wrinkles at a flame front close to the stability limits and in self-turbulization of the flame far from the limits. The self-turbulization can also be interpreted as a fractal structure. The fractal dimension of a flame front and velocity of a self-turbulized flame are evaluated. [S1063-651X(99)00809-0]

PACS number(s): 47.20.-k, 82.40.Py, 47.53.+n

I. INTRODUCTION

One of the most important issues in combustion science is the velocity of flame propagation [1,2]. While velocity of a planar flame U_f is determined by thermal and chemical fuel parameters, the resulting velocity of flame propagation U_w depends also on the flame shape: the more curved and wrinkled the flame front, the faster it propagates. In the absence of external turbulence a curved flame shape results from intrinsic flame instabilities such as the Darrieus-Landau (DL) instability inherent to any premixed flame in a gaseous fuel [3]. It follows from the linear theory of the DL instability that a planar flame front is bent by two-dimensional (2D) and three-dimensional (3D) perturbations, if the perturbation wavelength exceeds the cutoff wavelength λ_c determined by thermal conduction and finite flame thickness [4]. Typically, the cutoff wavelength is considerably larger than the flame thickness L_f and for most of the laboratory flames $\lambda_c > 20L_f$. Numerical simulations of flame dynamics in tubes of moderate width $\lambda_c/2 < R < 3\lambda_c/2$ with ideally adiabatic and slip walls have shown that at the nonlinear stage the DL instability results in a smooth curved stationary flame shape, which may be described as a hump directed towards the fuel and a cusp pointing to the burnt matter [5–7], see Fig. 1(a).

If we consider a tube width much larger than the cutoff wavelength, then the stabilizing influence of the curved shape weakens and a curved stationary flame presumably becomes unstable against perturbations of a small scale, much smaller than the curvature radius of the flame but larger than the cutoff wavelength. Qualitative description of such secondary DL instability may be found in [8], where the stabilizing influence of flame stretch on the development of

the secondary instability has been pointed out. In [8] stability of curved flames has been discussed in the scope of the model of an infinitely thin front, which implies infinite ratio of the tube width and the cutoff wavelength $R \gg \lambda_c$, as well as the strongly developed secondary DL instability. Obviously, such an extreme case must be separated from the case of tubes of moderate width $R < 3\lambda_c/2$ by a critical tube width R_w , so that for $R < R_w$ curved stationary flames are stable and for $R > R_w$ they become unstable. Qualitative estimates [8] give the critical tube width about $R_w = 5\lambda_c/2$ for flames with realistic ratio of the fuel density and the density of the burning products. Close to the stability limits the secondary instability may take the form of an extra cusp which develops at the hump of a stationary flame, as has been observed in 2D simulations [9]; see Fig. 1 (the flame front propagates to the left). Development of an extra cusp leads to additional amplification of the flame velocity in comparison with the velocity of a curved stationary flame.

Far away from the stability limits in very wide tubes, the secondary DL instability results in fractal structure of a flame front with many cascades of humps and cusps of different scales imposed one on another similar to the flames observed experimentally in [10]. As a matter of fact, development of the fractal structure has been interpreted in [10] as spontaneous turbulization of a flame front. The last interpretation is quite reasonable, since from the experimental point of view fractal flames do look like turbulent ones. In the case of self-turbulized flames velocity of flame propagation is determined by the tube width and by the fractal dimension of the flame front. To find the fractal dimension one has to know the increase of the flame velocity and of the linear size of the humps on every step of the fractal structure. A curved sta-

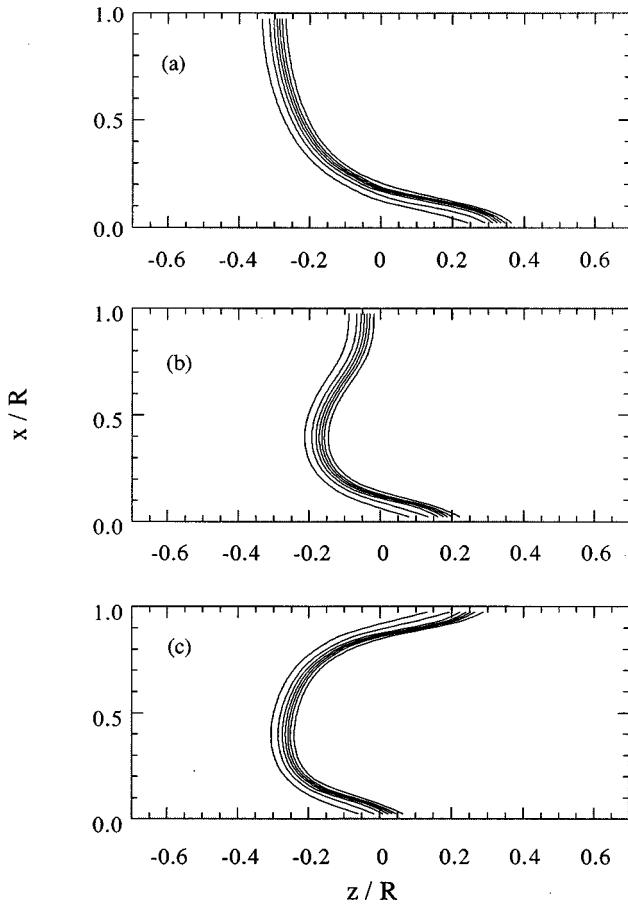


FIG. 1. Development of a curved flame front with an extra cusp observed in numerical simulations [9] in a tube with ideally adiabatic and slip walls. (a), (b), and (c) correspond to the time instants $U_f t / L_f = 78.8, 107.6, 379.8$ after the initiation of the DL instability at a planar flame front.

tionary flame may be considered as one step of the fractal structure at the flame front. Respectively, the fractal dimension of a flame front may be evaluated on the basis of the theory of dynamics and stability of curved stationary flames [11]. The velocity increase on one step of the fractal structure is given by the velocity amplification for curved stationary flames in comparison with planar ones. The increase of the linear size of the humps on one step of the fractal structure follows from stability limits of curved stationary flames. While the velocity amplification for curved stationary flames has been obtained both numerically [6,7] and analytically [12,13], the problem of stability limits is not solved yet.

For a long time dynamics of curved flames has been investigated on the basis of the nonlinear Sivashinsky equation [14] derived in the limit of small fuel expansion $\Theta - 1 \ll 1$, where Θ is defined as the ratio of the fuel density and the density of the burnt matter. Analytical solution of a 2D version of the nonlinear equation has been found in [15]. It has also been shown in [15] that the obtained curved stationary solutions are linearly stable against all perturbations of a small amplitude no matter how wide the ideal tube where the flame propagates is. This surprising result obviously contradicts the above physical ideas on the stability of a curved flame. In order to avoid the contradiction it was proposed in [16] that the curved stationary flames are linearly stable, but

nonlinearly unstable against perturbations of some finite amplitude. It was proposed also that the perturbation amplitude needed to induce the nonlinear instability goes to zero as the tube width goes to infinity. However, the critical tube width for which a curved stationary flame may become unstable could not be determined from the analysis [16].

When the Sivashinsky equation and its modifications have been used to study fractal flame structure researchers also faced a problem. Though in many works based on the nonlinear equation [14] flame shapes resembling fractal structure have been reported [17–21], still quite different values of flame fractal dimension have been found in different papers. It was even claimed in [19] that it is impossible to describe a fractal flame in the scope of the Sivashinsky equation. Indeed, if the fractal dimension depends on the expansion coefficient Θ of the flame as was shown in [19], then fractal flames cannot be obtained within the theory [14] since the Sivashinsky equation in a scaled form does not contain the expansion coefficient as a parameter.

Another shortcoming of the theory [14] is that the limit of small expansion coefficients $\Theta - 1 \ll 1$ for which the Sivashinsky equation has been derived is rather peculiar, being quite far from the case of realistic laboratory flames with $\Theta = 5 - 10$. To overcome this drawback, a nonlinear equation for a curved stationary flame of an arbitrary expansion coefficient has been derived in [12]. In the reference frame of a curved stationary flame $z = F(\mathbf{x}) - U_w t$ the nonlinear equation takes the form

$$1 - U_w / U_f + \frac{\Theta}{2} (\nabla F)^2 + \frac{(\Theta - 1)^3}{16\Theta} - [(\nabla F)^2 - (\hat{\Phi} F)^2] = \frac{\Theta - 1}{2} \left(\hat{\Phi} F + \frac{\lambda_c}{2\pi} \nabla^2 F \right), \quad (1)$$

where U_f is the velocity of a planar flame, the operator $\hat{\Phi}$ is defined as

$$\hat{\Phi} F = \frac{1}{4\pi^2} \int_{-\infty}^{\infty} |\mathbf{k}| F_{\mathbf{k}} \exp(i\mathbf{k} \cdot \mathbf{x}) d\mathbf{k}, \quad (2)$$

and $F_{\mathbf{k}}$ is the Fourier transform of F . The stationary nonlinear equation predicts quite well the velocity amplification of curved stationary flames both for the cases of 2D flames [12] and 3D flames in cylindrical tubes [13]. Particularly, the maximal possible velocity amplification for a 2D curved stationary flame predicted on the basis of Eq. (1),

$$U_m \equiv \max(U_w - U_f) = \frac{\Theta}{2} \frac{(\Theta - 1)^2}{\Theta^3 + \Theta^2 + 3\Theta - 1} U_f, \quad (3)$$

is in a very good agreement with the results of numerical simulations [6].

In the present paper we derive a time-dependent nonlinear equation for a nonstationary curved flame front of an arbitrary expansion coefficient under the assumptions of a small but finite flame thickness and weak nonlinearity. In the linear case of small perturbation amplitude the derived equation reproduces the dispersion relation for the perturbation growth rate [4]. For the case of stationary flames the derived equation goes over to the nonlinear equation (1) [12] and in

the limit of a small expansion coefficient $\Theta - 1 \ll 1$ it coincides with the Sivashinsky equation [14]. Linearizing the obtained equation around the stationary solutions [12] we investigate stability of a 2D curved stationary flame. Solution of the eigenvalue stability problem shows that the curved stationary flames become unstable for sufficiently wide tubes. The obtained stability limits are in a good agreement with the stability limits found in numerical simulations of flame dynamics [9] and in semiqualitative stability analysis of curved stationary flames [8]. Possible outcomes of the obtained instability at the nonlinear stage are discussed. The fractal dimension of self-turbulized flames is evaluated.

II. THE MODEL OF A THIN FLAME FRONT

We consider a 2D incompressible flow caused by a curved nonstationary flame propagating in an initially uniform fuel. A typical example of such a flame is a flame front in a tube of width R with ideally adiabatic and slip walls like that shown in Fig. 1. The fuel is assumed to be an ideal gas with a constant coefficient of thermal conduction and a constant specific heat; the fuel diffusion coefficient is equal to the coefficient of thermal diffusivity (Lewis number is equal to unity). We assume that there are no external sources of vorticity, so that the curved flame shape results from development of the DL instability. Since the DL instability is not affected by viscosity [6,12,22] we consider an inviscid flow $\text{Pr} = 0$. Typically flame thickness L_f is much less than the hydrodynamical length scale (e.g., the tube width R), so that a flame may be described in the scope of the discontinuity model of a thin flame front [4,23]. Though this model treats a flame as a discontinuity surface, the small but finite thickness is taken into account as an external parameter in the equation of flame evolution and in the conservation laws at the flame front. We shall use the evolution equation of a flame front and the conservation laws which have been derived in [4,23] in the limit of a small flame thickness $L_f/R \ll 1$. Particularly, in the case $\text{Le}=1$, $\text{Pr}=0$ evolution of a flame front $F(\mathbf{x},t)=0$ is described by the equation

$$\mathbf{n} \cdot \mathbf{v}_- + \frac{1}{N} \frac{\partial F}{\partial t} = U_f - L_f \frac{\Theta \ln \Theta}{\Theta - 1} \times \left(\frac{1}{N} \frac{\partial N}{\partial t} + \frac{1}{N} \nabla \cdot [N(\mathbf{v}_- - U_f \mathbf{n})] \right), \quad (4)$$

while the conservation laws may be written as

$$\rho \left(\mathbf{n} \cdot \mathbf{v} + \frac{1}{N} \frac{\partial F}{\partial t} \right) \Big|_{-}^{+} = \rho_- L_f \ln \Theta \times \left(\frac{1}{N} \frac{\partial N}{\partial t} + \frac{1}{N} \nabla \cdot [N(\mathbf{v}_- - U_f \mathbf{n})] \right), \quad (5)$$

$$\mathbf{n} \times \mathbf{v} \Big|_{-}^{+} = \frac{L_f \Theta \ln \Theta}{U_f} \mathbf{n} \times \hat{D}_t (\mathbf{v}_- - U_f \mathbf{n}), \quad (6)$$

$$\left[P + \rho \left(\mathbf{n} \cdot \mathbf{v} + \frac{1}{N} \frac{\partial F}{\partial t} \right)^2 \right] \Big|_{-}^{+} = -L_f \rho_- U_f^2 (\Theta - 1) \nabla \cdot \mathbf{n} + L_f \rho_- \Theta \ln \Theta \left(\frac{U_f}{N} \hat{D}_t N + \mathbf{n} \cdot \frac{\partial \mathbf{v}_-}{\partial t} + \mathbf{n} \cdot (\mathbf{v}_- \cdot \nabla) \mathbf{v}_- \right), \quad (7)$$

with the introduced operator $\hat{D}_t = \partial/\partial t + \mathbf{v}_- \cdot \nabla - U_f \mathbf{n} \cdot \nabla$. Here the labels $-$ and $+$ correspond to the flows just ahead and just behind the flame front, $\mathbf{n} = \nabla F/N$ is the unit normal vector directed to the burning products and the designation $N = |\nabla F|$ is introduced. The left-hand sides of Eqs. (5)–(7) are usual conservation laws at a surface of discontinuity of zero thickness [3], the right-hand sides of Eqs. (5)–(7) show the influence of thermal conduction and finite flame thickness on dynamics of a curved flame front. The unknown flow just ahead of the flame front results from flame evolution, so that \mathbf{v}_- in Eqs. (4)–(7) is some functional of F , which we have to find. To find the relation between \mathbf{v}_- and F we have to solve the equations of ideal hydrodynamics ahead and behind the flame front,

$$\nabla \cdot \mathbf{v} = 0, \quad (8)$$

$$\frac{\partial \mathbf{v}}{\partial t} + (\mathbf{v} \cdot \nabla) \mathbf{v} + \frac{1}{\rho} \nabla P = 0, \quad (9)$$

and match these solutions at the flame front of a small but finite thickness by use of the conservation laws.

It is convenient to introduce the dimensionless variables $(\eta; \xi) = (x/R; z/R)$, $\tau = U_f t/R$, $(w; u) = \mathbf{v}/U_f$, $\Pi = (P - P_f)/\rho_- U_f^2$, where P_f is the initial pressure of the fuel far ahead of the flame front at $z \rightarrow -\infty$. We introduce also the small parameter $\varepsilon = L_f/R \ll 1$, which characterizes the ratio of the flame thickness and the channel width. For the introduced variables the 2D equations of ideal hydrodynamics become

$$\frac{\partial u}{\partial \xi} + \frac{\partial w}{\partial \eta} = 0, \quad (10)$$

$$\frac{\partial w}{\partial \tau} + u \frac{\partial w}{\partial \xi} + w \frac{\partial w}{\partial \eta} = -\frac{1}{r} \frac{\partial \Pi}{\partial \eta}, \quad (11)$$

$$\frac{\partial u}{\partial \tau} + u \frac{\partial u}{\partial \xi} + w \frac{\partial u}{\partial \eta} = -\frac{1}{r} \frac{\partial \Pi}{\partial \xi}, \quad (12)$$

where the scaled density is $r=1$ for the fuel and $r=1/\Theta$ for the burnt matter. We consider a flow in the reference frame of the curved stationary flame moving with velocity U_w . It is convenient to introduce the scaled velocity of a curved stationary flame $W = U_w/U_f - 1$. Though we adopt an inertial reference frame of a stationary front, in general a flame front is not stationary and the evolution equation for a curved flame front $\xi = f(\eta, \tau)$ takes the form

$$\frac{\partial f}{\partial \tau} - u_- + w_- \frac{df}{d\eta} - N = \varepsilon \frac{\Theta \ln \Theta}{\Theta - 1} \left(\frac{\partial N}{\partial \tau} + \frac{d}{d\eta} (Nw_-) + \frac{d^2 f}{d\eta^2} \right), \quad (13)$$

where the value N in the 2D configuration becomes $N = \sqrt{1 + (df/d\eta)^2}$. Taking into account Eq. (13) the conservation laws at the flame front may be written as

$$u_+ - u_- - \frac{df}{d\eta} (w_+ - w_-) = (\Theta - 1)N, \quad (14)$$

$$w_+ - w_- + \frac{df}{d\eta} (u_+ - u_-) = \varepsilon \ln \Theta \left(\hat{D}_\tau w_- + \frac{df}{d\eta} \hat{D}_\tau u_- + \frac{1}{N} \hat{D}_\tau \frac{\partial f}{\partial \eta} \right), \quad (15)$$

$$\begin{aligned} & \Pi_+ + \frac{N^{-2}}{\Theta} \left(u_+ - \frac{\partial f}{\partial \eta} w_+ - \frac{\partial f}{\partial \tau} \right)^2 \\ & - \Pi_- - N^{-2} \left(u_- - \frac{\partial f}{\partial \eta} w_- - \frac{\partial f}{\partial \tau} \right)^2 \\ & = \varepsilon (\Theta - 1) \frac{\partial}{\partial \eta} \left(\frac{1}{N} \frac{\partial f}{\partial \eta} \right) + \frac{\varepsilon \ln \Theta}{N} \\ & \times \left(\frac{\partial^2 f}{\partial \tau^2} + 2w_- \frac{\partial^2 f}{\partial \tau \partial \eta} + w_-^2 \frac{\partial^2 f}{\partial \eta^2} + 2\hat{D}_\tau N - \frac{1}{N} \frac{\partial f}{\partial \eta} \frac{\partial N}{\partial \eta} \right), \end{aligned} \quad (16)$$

where

$$\hat{D}_\tau = \frac{\partial}{\partial \tau} + w_- \frac{\partial}{\partial \eta} + \frac{1}{N} \frac{\partial f}{\partial \eta} \frac{\partial}{\partial \eta}. \quad (17)$$

Since there are no other sources of vorticity except the curved flame itself, upstream of the flame front one has

$$\frac{\partial u}{\partial \eta} - \frac{\partial w}{\partial \xi} = 0, \quad (18)$$

and the velocity potential $u = \partial \varphi / \partial \xi$, $w = \partial \varphi / \partial \eta$ may be introduced for the upstream flow. Pressure in a potential flow is determined by Bernoulli's equation

$$\Pi = \frac{1}{2} (1 + W)^2 - \frac{1}{2} (u^2 + w^2) - \frac{\partial \varphi}{\partial \tau}. \quad (19)$$

In order to describe the vorticity flow behind the curved flame we introduce the stream function

$$u = \frac{\partial \psi}{\partial \eta}, \quad w = -\frac{\partial \psi}{\partial \xi}, \quad (20)$$

which obeys the equation

$$\left(\frac{\partial}{\partial t} + \mathbf{v} \cdot \nabla \right) \nabla^2 \psi = 0 \quad (21)$$

describing vorticity drift by the flow.

In the above statement of the problem a planar flame front corresponds to $f=0$, $W=0$. The fuel flows towards the planar front with the velocity $u=1$, $w=0$ and the burnt matter is drifted away with the velocity $u=\Theta$, $w=0$. As the fuel passes the planar flame, the density of the burning matter changes from $r=1$ to $r=1/\Theta$ and the scaled pressure drops from $\Pi=0$ to $\Pi=-\Theta+1$.

III. THE NONLINEAR EQUATION FOR A CURVED NONSTATIONARY FLAME

We are going to derive the nonlinear equation describing dynamics of a curved nonstationary flame under the assumptions of a thin flame front $\varepsilon \ll 1$ and weak nonlinearity. These assumptions have been employed in the derivation of the stationary nonlinear equation Eq. (1) and proved to be a success. Besides, the assumption of a thin flame front was used in the discontinuity model Eqs. (4)–(7), so that it is the only justified approach to the formulated problem.

It is convenient to distinguish the nonstationary components of all flow parameters by introducing the following variables for the flow ahead of the flame front:

$$u = 1 + W + \tilde{u}, \quad w = \tilde{w}, \quad \Pi = \tilde{\Pi}, \quad \varphi = (1 + W)\xi + \tilde{\varphi} \quad (22)$$

and for the flow behind the flame:

$$u = \Theta + W + \tilde{u}, \quad w = \tilde{w}, \quad \Pi = -\Theta + 1 + \tilde{\Pi}, \quad \psi = (\Theta + W)\eta + \tilde{\psi}. \quad (23)$$

By order of magnitude the scaled velocity of a curved stationary flame is $W \propto (\partial f / \partial \eta)^2$. Since the flow ahead of the flame front is potential, then the solution for the velocity components in the incoming flow is

$$\tilde{u} = \frac{1}{2\pi} \int_{-\infty}^{+\infty} \tilde{u}_k \exp(|K|\xi + iK\eta) dK, \quad (24)$$

$$\tilde{w} = \hat{\Phi}^{-1} \frac{\partial \tilde{u}}{\partial \eta}, \quad (25)$$

$$\tilde{\varphi} = \hat{\Phi}^{-1} \tilde{u}. \quad (26)$$

For the scaled variables the operator $\hat{\Phi}$ implies multiplication by the absolute value of the scaled wave number $K = kR$ in the Fourier space, while the inverse operator corresponds to division by the absolute value of the wave number. Obviously, for the inverse operator one has the identity $\hat{\Phi}^{-1} \hat{\Phi} f = f$. Pressure in the incoming flow follows from the Bernoulli equation, which takes the following form in the approximation of the second order nonlinearity:

$$\tilde{\Pi} = -\frac{\partial \tilde{\varphi}}{\partial \tau} - \tilde{u} - \frac{1}{2} (\tilde{u}^2 + \tilde{w}^2). \quad (27)$$

Keeping only the nonlinear terms of the second order and taking into account the condition of the small flame thickness $\varepsilon \ll 1$ we can rewrite the conservation laws at the flame front as

$$\tilde{u}_+ - \tilde{u}_- - (\tilde{w}_+ - \tilde{w}_-) \frac{\partial f}{\partial \eta} = \frac{\Theta - 1}{2} \left(\frac{\partial f}{\partial \eta} \right)^2, \quad (28)$$

$$\tilde{w}_+ - \tilde{w}_- + (\Theta - 1) \frac{\partial f}{\partial \eta} = \varepsilon \ln \Theta \left(\frac{\partial \tilde{w}_-}{\partial \tau} + \frac{\partial^2 f}{\partial \tau \partial \eta} \right), \quad (29)$$

$$\tilde{\Pi}_+ - \tilde{\Pi}_- - \frac{\Theta - 1}{\Theta} \left(\tilde{u}_- - \frac{\partial f}{\partial \tau} \right)^2 = \varepsilon (\Theta - 1) \frac{\partial^2 f}{\partial \eta^2} + \varepsilon \ln \Theta \frac{\partial^2 f}{\partial \tau^2}. \quad (30)$$

With the same accuracy the evolution equation for the flame front becomes

$$\frac{\partial f}{\partial \tau} + \tilde{w}_- \frac{\partial f}{\partial \eta} - \tilde{u}_- - W + \frac{1}{2} \left(\frac{\partial f}{\partial \eta} \right)^2 = \varepsilon \frac{\Theta \ln \Theta}{\Theta - 1} \left(\frac{\partial \tilde{w}_-}{\partial \eta} + \frac{\partial^2 f}{\partial \eta^2} \right). \quad (31)$$

A. First order approximation

In the first order approximation we take into account the first order terms in perturbations for an infinitely thin front ($\varepsilon=0$). In this approximation parameters of the incoming flow satisfy the relations

$$\tilde{w}_- = \hat{\Phi}^{-1} \frac{\partial \tilde{u}_-}{\partial \eta}, \quad (32)$$

$$\tilde{\Pi}_- = -\tilde{u}_- - \hat{\Phi}^{-1} \frac{\partial \tilde{u}_-}{\partial \tau}, \quad (33)$$

while the conservation laws at the flame front take the form

$$\tilde{u}_+ = \tilde{u}_-, \quad \tilde{w}_+ = \tilde{w}_- - (\Theta - 1) \frac{\partial f}{\partial \eta}, \quad \tilde{\Pi}_+ = \tilde{\Pi}_-. \quad (34)$$

In the linear approximation Eq. (21) can be rewritten as

$$\left(\frac{\partial}{\partial \tau} + \Theta \frac{\partial}{\partial \xi} \right) \nabla^2 \tilde{\psi} = 0. \quad (35)$$

Any solution to Eq. (35) may be presented as a sum of the potential mode $\tilde{\psi}_p$ and the vorticity mode $\tilde{\psi}_v$. The potential mode satisfies the relations

$$\nabla^2 \tilde{\psi}_p = 0, \quad (36)$$

$$\tilde{u}_p = \frac{1}{2\pi} \int_{-\infty}^{+\infty} \tilde{u}_{pk} \exp(-|K|\xi + iK\eta) dK, \quad (37)$$

$$\tilde{w}_p = -\hat{\Phi}^{-1} \frac{\partial \tilde{u}_p}{\partial \eta}, \quad (38)$$

$$\tilde{\Pi}_p = -\tilde{u}_p + \frac{1}{\Theta} \hat{\Phi}^{-1} \frac{\partial \tilde{u}_p}{\partial \tau}, \quad (39)$$

while for the vorticity mode one has

$$\left(\frac{\partial}{\partial \tau} + \Theta \frac{\partial}{\partial \xi} \right) \tilde{\psi}_v = 0, \quad (40)$$

$$\frac{1}{\Theta} \frac{\partial \tilde{u}_v}{\partial \tau} = \frac{\partial \tilde{w}_v}{\partial \eta}, \quad (41)$$

$$\tilde{\Pi}_v = 0. \quad (42)$$

Taking into account that $\tilde{u}_v = \tilde{u} - \tilde{u}_p$, $\tilde{w}_v = \tilde{w} - \tilde{w}_p$, $\tilde{\Pi} = \tilde{\Pi}_p$, we get the equation for the variables in the downstream flow in the first order of approximation

$$\hat{\Phi} \tilde{\Pi} + \frac{\partial \tilde{w}}{\partial \eta} - \frac{1}{\Theta} \frac{\partial \tilde{u}}{\partial \tau} = 0. \quad (43)$$

Substituting Eqs. (32)–(34) into Eq. (43), we have the following linear relation between perturbations of the flame front and the velocity perturbations just ahead of the flame front:

$$\tilde{u}_- + \frac{\Theta + 1}{2\Theta} \hat{\Phi}^{-1} \frac{\partial \tilde{u}_-}{\partial \tau} = \frac{\Theta - 1}{2} \hat{\Phi} f. \quad (44)$$

Another relation of these two values follows from the evolution equation (31), which becomes in the first order approximation

$$\tilde{u}_- = \frac{\partial f}{\partial \tau}. \quad (45)$$

The linear equation for flame front perturbations is obtained by substituting \tilde{u}_- from Eq. (45) into Eq. (44):

$$\frac{\Theta + 1}{2\Theta} \hat{\Phi}^{-1} \frac{\partial^2 f}{\partial \tau^2} + \frac{\partial f}{\partial \tau} - \frac{\Theta - 1}{2} \hat{\Phi} f = 0. \quad (46)$$

The above equation gives the same dispersion relation for the perturbation growth rate as that of the DL instability for an infinitely thin flame front in the linear approximation [3]. The nonlinear equation for a flame front of finite thickness is the next order approximation. In order to find the nonlinear equation it is convenient to introduce a function ϕ as

$$\tilde{u}_- = \frac{\Theta - 1}{2} \left\{ \hat{\Phi} \phi + \varepsilon \frac{\partial^2 \phi}{\partial \eta^2} - \frac{(\Theta - 1)^2}{8\Theta} \left[\left(\frac{\partial \phi}{\partial \eta} \right)^2 - (\hat{\Phi} \phi)^2 \right] \right\} \quad (47)$$

and the following designation:

$$A = \frac{\Theta + 1}{2\Theta} \hat{\Phi}^{-1} \frac{\partial \phi}{\partial \tau}. \quad (48)$$

In the case of the curved stationary flames [12] the relation Eq. (47) couples the velocity perturbation \tilde{u}_- and the flame front position f .

For the introduced function one has in the first order of approximation

$$f = \phi + A, \quad (49)$$

$$\tilde{u}_- = \frac{\Theta - 1}{2} \hat{\Phi} \phi, \quad (50)$$

$$\tilde{w}_- = \frac{\Theta - 1}{2} \frac{\partial \phi}{\partial \eta}, \quad (51)$$

$$\tilde{\Pi}_- = -\frac{\Theta - 1}{2} \left(\frac{\partial \phi}{\partial \tau} + \hat{\Phi} \phi \right), \quad (52)$$

$$\tilde{u}_+ = \tilde{u}_-, \quad \tilde{\Pi}_+ = \tilde{\Pi}_-, \quad (53)$$

$$\tilde{w}_+ = -\tilde{w}_- - (\Theta - 1) \frac{\partial A}{\partial \eta}, \quad (54)$$

$$\frac{\partial A}{\partial \tau} + \frac{\partial \phi}{\partial \tau} = \frac{\Theta - 1}{2} \hat{\Phi} \phi. \quad (55)$$

B. Second order approximation

In the second order approximation we take into account the second order terms in perturbations and first order terms in perturbations proportional to the small flame thickness $\varepsilon \ll 1$. Though we are interested in the nonlinear equation for the flame front position f , it is easier to perform calculations with respect to the artificially introduced function ϕ , Eq. (47). In the second order approximation we can rewrite the evolution equation (31) in the form

$$\begin{aligned} -W + \frac{\partial f}{\partial \tau} + \frac{\Theta}{2} \left(\frac{\partial \phi}{\partial \eta} \right)^2 + \frac{(\Theta - 1)^3}{16\Theta} \left[\left(\frac{\partial \phi}{\partial \eta} \right)^2 - (\hat{\Phi} \phi)^2 \right] \\ + \frac{\Theta + 1}{2} \frac{\partial \phi}{\partial \eta} \frac{\partial A}{\partial \eta} + \frac{1}{2} \left(\frac{\partial A}{\partial \eta} \right)^2 = \frac{\Theta - 1}{2} \hat{\Phi} \phi \\ + \frac{\varepsilon}{2} \left[\Theta \ln \Theta \frac{\Theta + 1}{\Theta - 1} + \Theta - 1 \right] \frac{\partial^2 \phi}{\partial \eta^2} - \frac{\varepsilon \ln \Theta}{2} \frac{\Theta + 1}{\Theta - 1} \hat{\Phi} \frac{\partial \phi}{\partial \tau}. \end{aligned} \quad (56)$$

For a curved stationary flame front one has

$$f = f(\eta), \quad \phi = \phi(\eta), \quad W = U_w / U_f - 1, \quad A = 0, \quad (57)$$

and Eq. (56) coincides with the scaled nonlinear stationary equation (1) derived in [12]:

$$\begin{aligned} 1 - U_w / U_f + \frac{\Theta}{2} \left(\frac{\partial \phi}{\partial \eta} \right)^2 + \frac{(\Theta - 1)^3}{16\Theta} \left[\left(\frac{\partial \phi}{\partial \eta} \right)^2 - (\hat{\Phi} \phi)^2 \right] \\ = \frac{\Theta - 1}{2} \hat{\Phi} \phi + \frac{\varepsilon}{2} \left(\Theta \ln \Theta \frac{\Theta + 1}{\Theta - 1} + \Theta - 1 \right) \frac{\partial^2 \phi}{\partial \eta^2}. \end{aligned} \quad (58)$$

In the case of a curved stationary flame the introduced function ϕ plays the role of the flame front position, while in a general nonstationary case the difference between the function ϕ and the flame front position is related to time-dependent terms. In order to solve the problem of flame dynamics we have to complement the evolution equation (56) with the nonlinear nonstationary equation, which relates the flame front position f to the function ϕ . In the second order approximation the solution just ahead of the flame front may be written as

$$\tilde{u}_- = \tilde{u}_{0-} - \frac{\Theta - 1}{2} (\phi + A) \frac{\partial^2 \phi}{\partial \eta^2}, \quad (59)$$

$$\tilde{w}_- = \hat{\Phi}^{-1} \frac{\partial \tilde{u}_{0-}}{\partial \eta} + \frac{\Theta - 1}{2} (\phi + A) \hat{\Phi} \frac{\partial \phi}{\partial \eta}, \quad (60)$$

$$\begin{aligned} \tilde{\Pi}_- = -\hat{\Phi}^{-1} \frac{\partial \tilde{u}_{0-}}{\partial \tau} - \tilde{u}_{0-} - \frac{\Theta - 1}{2} (\phi + A) \hat{\Phi} \frac{\partial \phi}{\partial \tau} \\ + \frac{\Theta - 1}{2} (\phi + A) \frac{\partial^2 \phi}{\partial \eta^2} - \frac{1}{2} (\tilde{u}_-^2 + \tilde{w}_-^2). \end{aligned} \quad (61)$$

Within the same accuracy the solution just behind the flame front takes the form

$$\tilde{u}_+ = \tilde{u}_{0+} + \frac{\Theta - 1}{2} (\phi + A) \frac{\partial^2 \phi}{\partial \eta^2} + (\Theta - 1) (\phi + A) \frac{\partial^2 A}{\partial \eta^2}, \quad (62)$$

$$\begin{aligned} \tilde{w}_+ = \tilde{w}_{0+} + \frac{\Theta - 1}{2} (\phi + A) \hat{\Phi} \frac{\partial \phi}{\partial \eta} + \frac{\Theta - 1}{\Theta} (\phi + A) \\ \times \frac{\partial^2}{\partial \tau \partial \eta} \left(\frac{\Theta + 1}{2} \phi + A \right), \end{aligned} \quad (63)$$

$$\tilde{\Pi}_+ = \tilde{\Pi}_{0+} + \frac{\Theta - 1}{2} (\phi + A) \hat{\Phi} \frac{\partial \phi}{\partial \tau} - \frac{\Theta - 1}{2} (\phi + A) \frac{\partial^2 \phi}{\partial \eta^2}. \quad (64)$$

In the second order approximation the conservation laws Eqs. (28)–(30) give the following expressions for \tilde{u}_{0+} , \tilde{w}_{0+} , $\tilde{\Pi}_{0+}$:

$$\tilde{u}_{0+} = \tilde{u}_{0-} - (\Theta - 1) f \frac{\partial^2 f}{\partial \eta^2} - \frac{\Theta - 1}{2} \left(\frac{\partial f}{\partial \eta} \right)^2, \quad (65)$$

$$\begin{aligned} \tilde{w}_{0+} = \hat{\Phi}^{-1} \frac{\partial \tilde{u}_{0-}}{\partial \eta} - (\Theta - 1) \frac{\partial f}{\partial \eta} + \varepsilon \ln \Theta \left(\frac{\partial \tilde{w}_-}{\partial \tau} + \frac{\partial^2 f}{\partial \tau \partial \eta} \right) \\ - \frac{\Theta - 1}{\Theta} (\phi + A) \frac{\partial^2}{\partial \tau \partial \eta} \left(\frac{\Theta + 1}{2} \phi + A \right), \end{aligned} \quad (66)$$

$$\begin{aligned} \tilde{\Pi}_{0+} = -\hat{\Phi}^{-1} \frac{\partial \tilde{u}_{0-}}{\partial \tau} - \tilde{u}_{0-} - (\Theta - 1) (\phi + A) \hat{\Phi} \frac{\partial \phi}{\partial \tau} + (\Theta - 1) \\ \times (\phi + A) \frac{\partial^2 \phi}{\partial \eta^2} - \frac{1}{2} (\tilde{u}_-^2 + \tilde{w}_-^2) - \frac{\Theta - 1}{\Theta} \left(\tilde{u}_- - \frac{\partial f}{\partial \tau} \right)^2 \\ + \varepsilon (\Theta - 1) \frac{\partial^2 f}{\partial \eta^2} + \varepsilon \ln \Theta \frac{\partial^2 f}{\partial \tau^2}. \end{aligned} \quad (67)$$

The equation for the stream function in the downstream flow of burnt matter within the accuracy of the second order nonlinearity may be written as

$$\left(\frac{\partial}{\partial \tau} + \Theta \frac{\partial}{\partial \xi} \right) \nabla^2 \tilde{\psi} = - \left(\tilde{u} \frac{\partial}{\partial \xi} + \tilde{w} \frac{\partial}{\partial \eta} \right) \nabla^2 \tilde{\psi}_v. \quad (68)$$

In this approximation Eq. (68) is a linear equation with constant coefficients and the known right-hand side defined by solutions (38)–(42). Obviously, the general solution of Eq. (68) is a superposition of the potential mode $\tilde{\psi}_p$, Eqs. (36)–(39), of the vorticity mode $\tilde{\psi}_v$, Eqs. (40)–(42), and any particular solution $\tilde{\psi}_a$ of Eq. (68). Therefore, in order to find the solution in the downstream flow one needs to construct any particular solution of Eq. (68). Taking into account the continuity equation for the perturbed velocity $\nabla \cdot \tilde{\mathbf{u}} = 0$ we can rewrite Eq. (68) in the form

$$\left(\frac{\partial}{\partial \tau} + \Theta \frac{\partial}{\partial \xi} \right) \nabla^2 \tilde{\psi}_a = -\nabla \cdot (\tilde{\mathbf{u}} \nabla^2 \tilde{\psi}_v). \quad (69)$$

For example, we may choose a particular solution $\tilde{\psi}_a$ that satisfies the equation

$$\left(\frac{\partial}{\partial \tau} + \Theta \frac{\partial}{\partial \xi} \right) \nabla \tilde{\psi}_a = -\tilde{\mathbf{u}} \nabla^2 \tilde{\psi}_v, \quad (70)$$

which may also be written in components as

$$\frac{\partial \tilde{u}_a}{\partial \tau} + \Theta \frac{\partial \tilde{u}_a}{\partial \xi} + \tilde{w} \left(\frac{\partial \tilde{u}_v}{\partial \eta} + \frac{1}{\Theta} \frac{\partial \tilde{w}_v}{\partial \tau} \right) = 0, \quad (71)$$

$$\frac{\partial \tilde{w}_a}{\partial \tau} + \Theta \frac{\partial \tilde{w}_a}{\partial \xi} - \tilde{u} \left(\frac{\partial \tilde{u}_v}{\partial \eta} + \frac{1}{\Theta} \frac{\partial \tilde{w}_v}{\partial \tau} \right) = 0. \quad (72)$$

Taking into account Eqs. (11),(72), and the structure of the potential and vorticity modes Eqs. (36)–(42) one comes to the equation

$$\left(\frac{\partial}{\partial \tau} + \Theta \frac{\partial}{\partial \xi} \right) \tilde{w}_p + \frac{\partial}{\partial \eta} \left(\Theta \tilde{\Pi} + \frac{\tilde{u}^2}{2} + \frac{\tilde{w}^2}{2} \right) = 0. \quad (73)$$

Substituting Eqs. (38),(72) into Eq. (73) we obtain the equation for the variables in the downstream flow,

$$\frac{\partial \tilde{u}}{\partial \tau} - \Theta \frac{\partial \tilde{w}}{\partial \eta} - \hat{\Phi} \left(\Theta \tilde{\Pi} + \frac{\tilde{u}^2}{2} + \frac{\tilde{w}^2}{2} \right) + \tilde{w} \left(\frac{\partial \tilde{u}_v}{\partial \eta} + \frac{1}{\Theta} \frac{\partial \tilde{w}_v}{\partial \tau} \right) = 0, \quad (74)$$

which can also be presented in the form

$$\frac{\partial \tilde{u}}{\partial \tau} - \Theta \frac{\partial \tilde{w}}{\partial \eta} - \hat{\Phi} \left(\Theta \tilde{\Pi} + \frac{\tilde{u}^2}{2} + \frac{\tilde{w}^2}{2} \right) + \tilde{w} \left(\frac{\partial \tilde{u}}{\partial \eta} + \frac{1}{\Theta} \frac{\partial \tilde{w}}{\partial \tau} + \frac{\partial \tilde{\Pi}}{\partial \eta} \right) = 0. \quad (75)$$

In the linear approximation the obtained condition in the downstream flow goes over to Eq. (43).

As soon as the condition in the downstream is found the desired nonlinear equation follows from the upstream conditions Eqs. (59)–(61), the conservation laws (65)–(67), and the downstream condition Eq. (75). Substituting $\tilde{u}_{0+}, \tilde{w}_{0+}, \tilde{\Pi}_{0+}$ from Eqs. (65)–(67) into Eq. (75) one has

$$\begin{aligned} & (\Theta + 1) \frac{\partial \tilde{u}_{0-}}{\partial \tau} + 2\Theta \hat{\Phi} \tilde{u}_{0-} + \Theta(\Theta - 1) \frac{\partial^2 f}{\partial \eta^2} - \varepsilon \Theta \ln \Theta \left(\frac{\partial^2 \tilde{w}_-}{\partial \tau \partial \eta} + \frac{\partial^3 f}{\partial \tau \partial \eta^2} \right) - \varepsilon \Theta(\Theta - 1) \hat{\Phi} \frac{\partial^2 f}{\partial \eta^2} - \varepsilon \Theta \ln \Theta \hat{\Phi} \frac{\partial^2 f}{\partial \tau^2} + (\Theta - 1) \hat{\Phi} \\ & \times \left[\Theta f \hat{\Phi} \frac{\partial \phi}{\partial \tau} - \Theta f \frac{\partial^2 \phi}{\partial \eta^2} + \frac{1}{2} (\tilde{w}_-^2 - \tilde{u}_-^2) + \frac{\partial f}{\partial \tau} \left(2\tilde{u}_{0-} - \frac{\partial f}{\partial \tau} \right) - \frac{\Theta - 1}{2} \frac{\partial A}{\partial \eta} \frac{\partial f}{\partial \eta} \right] - (\Theta - 1) \frac{\partial}{\partial \tau} \left(f \frac{\partial^2 f}{\partial \eta^2} \right) - \frac{\Theta - 1}{2} \frac{\partial}{\partial \tau} \left(\frac{\partial f}{\partial \eta} \right)^2 \\ & + \frac{(\Theta - 1)^2}{2} \frac{\partial}{\partial \eta} \left[f \left(\frac{\partial^2 \phi}{\partial \tau \partial \eta} + \hat{\Phi} \frac{\partial \phi}{\partial \eta} \right) \right] + \frac{(\Theta - 1)^3}{4\Theta} \left(\frac{\partial \phi}{\partial \eta} + 2 \frac{\partial A}{\partial \eta} \right) \left(\frac{\partial^2 \phi}{\partial \tau \partial \eta} + \hat{\Phi} \frac{\partial \phi}{\partial \eta} \right) = 0. \end{aligned} \quad (76)$$

According to the definition of ϕ , Eq. (47), one finds

$$\tilde{u}_{0-} = \frac{\Theta - 1}{2} \hat{\Phi} \phi + \frac{\Theta - 1}{2} (\phi + A) \frac{\partial^2 \phi}{\partial \eta^2} + \varepsilon \frac{\Theta - 1}{2} \frac{\partial^2 \phi}{\partial \eta^2} - \frac{\Theta - 1}{4\Theta} (\tilde{w}_-^2 - \tilde{u}_-^2). \quad (77)$$

Finally, substituting \tilde{u}_{0-} into Eq. (76) one comes to an equation relating position of the flame front f and the introduced function ϕ ,

$$\begin{aligned} & \Theta \frac{\partial^2}{\partial \eta^2} (f - \phi - A) + \varepsilon \frac{\Theta \ln \Theta}{\Theta - 1} \frac{\partial}{\partial \tau} \left(\frac{\Theta + 1}{2\Theta} \hat{\Phi} \frac{\partial \phi}{\partial \tau} - \frac{\partial^2 \phi}{\partial \eta^2} \right) + (\Theta - 1)^2 \frac{\Theta + 1}{16\Theta} \frac{\partial}{\partial \tau} \left[(\hat{\Phi} \phi)^2 - \left(\frac{\partial \phi}{\partial \eta} \right)^2 \right] \\ & + \frac{\partial}{\partial \eta} \left[(\phi + A) \frac{\partial^2}{\partial \tau \partial \eta} \left(\frac{\Theta + 1}{2} \phi + A \right) \right] + \frac{\Theta - 1}{2\Theta} \left(\frac{\partial \phi}{\partial \eta} + 2 \frac{\partial A}{\partial \eta} \right) \frac{\partial^2}{\partial \tau \partial \eta} \left(\frac{\Theta + 1}{2} \phi + A \right) + \frac{\partial}{\partial \tau} \left[(\phi + A) \frac{\partial^2}{\partial \eta^2} \left(\frac{\Theta - 1}{2} \phi - A \right) \right. \\ & \left. - \frac{1}{2} \left(\frac{\partial \phi}{\partial \eta} + \frac{\partial A}{\partial \eta} \right)^2 \right] + \hat{\Phi} \left[-\frac{\Theta - 1}{2} \left(\frac{\partial A}{\partial \eta} \right)^2 - \frac{\Theta - 1}{2} \frac{\partial \phi}{\partial \eta} \frac{\partial A}{\partial \eta} + \Theta (\phi + A) \hat{\Phi} \frac{\partial \phi}{\partial \tau} + \left(\frac{\partial \phi}{\partial \tau} + \frac{\partial A}{\partial \tau} \right)^2 \right] = 0. \end{aligned} \quad (78)$$

Equation (56) complemented by Eq. (78) determines evolution of a curved nonstationary flame front with the accuracy of second order nonlinearity. Together Eqs. (56),(78) may be written in the form of a single equation as

$$\frac{\partial^2}{\partial \eta^2} \Psi_0 - \Psi_1 = 0, \quad (79)$$

where the first term Ψ_0 is the combination of the linear dispersion relation for a flame front of finite thickness [4] and the nonlinear stationary equation (1),

$$\begin{aligned} \Psi_0 = & \frac{\Theta + 1}{2\Theta} \hat{\Phi}^{-1} \frac{\partial^2 \phi}{\partial \tau^2} + \left(1 + \varepsilon \frac{\Theta \ln \Theta}{\Theta - 1} \hat{\Phi} \right) \frac{\partial \phi}{\partial \tau} - W + \frac{\Theta}{2} \left(\frac{\partial \phi}{\partial \eta} \right)^2 + \frac{(\Theta - 1)^3}{16\Theta} \left[\left(\frac{\partial \phi}{\partial \eta} \right)^2 - (\hat{\Phi} \phi)^2 \right] \\ & - \frac{\Theta - 1}{2} \left(\hat{\Phi} \phi + \frac{\lambda_c}{2\pi R} \frac{\partial^2 \phi}{\partial \eta^2} \right). \end{aligned} \quad (80)$$

The second term Ψ_1 in Eq. (79) represents the nonlinear time-dependent part of the equation

$$\begin{aligned} \Psi_1 = & -\frac{1}{2} \frac{\partial^2}{\partial \eta^2} \left[(\Theta + 1) \frac{\partial \phi}{\partial \eta} \frac{\partial A}{\partial \eta} + \left(\frac{\partial A}{\partial \eta} \right)^2 \right] + (\Theta - 1)^2 \frac{\Theta + 1}{16\Theta^2} \frac{\partial^2}{\partial \tau^2} \left[(\hat{\Phi} \phi)^2 - \left(\frac{\partial \phi}{\partial \eta} \right)^2 \right] + \frac{\Theta - 1}{2\Theta} \frac{\partial}{\partial \tau} \left[\frac{\partial^2 \phi}{\partial \tau \partial \eta} \left(\frac{\partial \phi}{\partial \eta} + \frac{\partial A}{\partial \eta} \right) \right] \\ & + \hat{\Phi} \phi \frac{\partial^2}{\partial \eta^2} \left(\frac{\Theta - 1}{2} \phi - A \right) + \frac{\partial}{\partial \tau} \left[(\phi + A) \frac{\partial^3 \phi}{\partial \tau \partial \eta^2} \right] + \frac{(\Theta - 1)^2}{4\Theta^2} \frac{\partial}{\partial \tau} \left[\left(\frac{\partial \phi}{\partial \eta} + 2 \frac{\partial A}{\partial \eta} \right) \frac{\partial}{\partial \eta} \left(\frac{\partial \phi}{\partial \tau} + \hat{\Phi} \phi \right) \right] \\ & + \hat{\Phi} \frac{\partial}{\partial \tau} \left[\frac{(\Theta - 1)^2}{4\Theta} (\hat{\Phi} \phi)^2 + (\phi + A) \hat{\Phi} \frac{\partial \phi}{\partial \tau} - \frac{\Theta - 1}{2\Theta} \frac{\partial A}{\partial \eta} \left(\frac{\partial \phi}{\partial \eta} + \frac{\partial A}{\partial \eta} \right) \right]. \end{aligned} \quad (81)$$

The designation A stands for the combination $A = (\Theta + 1)/2\Theta \hat{\Phi}^{-1} \partial \phi / \partial \tau$, Eq. (48), and the flame front position f is calculated from the introduced function ϕ by use of Eq. (78). Time derivatives in nonlinear terms and in linear terms proportional to the scaled flame thickness ε of Eq. (81) were reduced taking into account the linear relation (55). The dimensional form of the nonlinear equation for a curved flame front $z = F(x, t) - U_w t$ is recovered from Eq. (79) by substitution of the expressions for the scaled variables $\eta = x/R$, $\tau = U_f t/R$, for the scaled wave number $K = kR$ in the operator $\hat{\Phi}$, for the parameter $\varepsilon = L_f/R$ characterizing flame thickness, for the scaled flame front position $f = F/R$, and for the introduced function $\phi = F_\phi/R$. The resulting dimensional nonlinear equation does not contain the hydrodynamical length scale R . In order to go over to a 3D configuration one can replace the spatial derivative $\partial/\partial x$ in Eq. (79) by ∇ and the absolute value of the wave number $|k|$ in the operator $\hat{\Phi}$ by $|\mathbf{k}|$. For example, the expression for the first term Ψ_0 of Eq. (79) in a 3D configuration for dimensional variables takes the form

$$\begin{aligned} \Psi_0 = & \frac{\Theta + 1}{2\Theta} \hat{\Phi}^{-1} \frac{1}{U_f^2} \frac{\partial^2 F_\phi}{\partial t^2} + \left(1 + L_f \frac{\Theta \ln \Theta}{\Theta - 1} \hat{\Phi} \right) \frac{1}{U_f} \frac{\partial F_\phi}{\partial t} + 1 \\ & - \frac{U_w}{U_f} + \frac{\Theta}{2} (\nabla F_\phi)^2 + \frac{(\Theta - 1)^3}{16\Theta} [(\nabla F_\phi)^2 - (\hat{\Phi} F_\phi)^2] \\ & - \frac{\Theta - 1}{2} \left(\hat{\Phi} F_\phi + \frac{\lambda_c}{2\pi} \nabla^2 F_\phi \right). \end{aligned} \quad (82)$$

In the linear case of a slightly perturbed flame front the nonlinear equation (79) goes over to the equation describing the linear stage of the DL instability at a planar flame of finite

thickness derived in Ref. [4], with $\text{Le} = 1$ and constant coefficient of thermal conduction

$$\begin{aligned} \frac{\Theta + 1}{2\Theta} \hat{\Phi}^{-1} \frac{\partial^2 \phi}{\partial \tau^2} + \left(1 + \varepsilon \frac{\Theta \ln \Theta}{\Theta - 1} \hat{\Phi} \right) \frac{\partial \phi}{\partial \tau} \\ - \frac{\Theta - 1}{2} \left(\hat{\Phi} \phi + \frac{\lambda_c}{2\pi R} \frac{\partial^2 \phi}{\partial \eta^2} \right) = 0. \end{aligned} \quad (83)$$

For a curved stationary flame front Eq. (79) is consistent with Eq. (1) and, finally, in the limit of a small expansion coefficient $\Theta - 1 \ll 1$ time evolution of a flame front becomes slow, $\partial \phi / \partial \tau \propto u(\Theta - 1)\phi$, and Eq. (79) goes over to the Sivashinsky equation [14].

Though in the present paper the nonlinear equation (79) for a curved flame front has been derived for $\text{Le} = 1$, nonviscous flow, and constant coefficient of thermal conduction, this equation is also applicable to a flame in a viscous fuel with an arbitrary dependence of the transport coefficients on temperature and any Lewis number, for which the thermal-diffusion instability does not occur. These corrections lead only to certain changes of the coefficients in front of the linear terms in Eq. (80) that may be written as

$$\begin{aligned} \Psi_0 = & \frac{\Theta + 1}{2\Theta} (1 + \varepsilon C_1 \hat{\Phi}) \hat{\Phi}^{-1} \frac{\partial^2 \phi}{\partial \tau^2} + (1 + \varepsilon C_2 \hat{\Phi}) \frac{\partial \phi}{\partial \tau} \\ & + 1 - U_w/U_f + \frac{\Theta}{2} \left(\frac{\partial \phi}{\partial \eta} \right)^2 + \frac{(\Theta - 1)^3}{16\Theta} \left[\left(\frac{\partial \phi}{\partial \eta} \right)^2 - (\hat{\Phi} \phi)^2 \right] \\ & - \frac{\Theta - 1}{2} (1 - \varepsilon C_3 \hat{\Phi}) \hat{\Phi} \phi. \end{aligned} \quad (84)$$

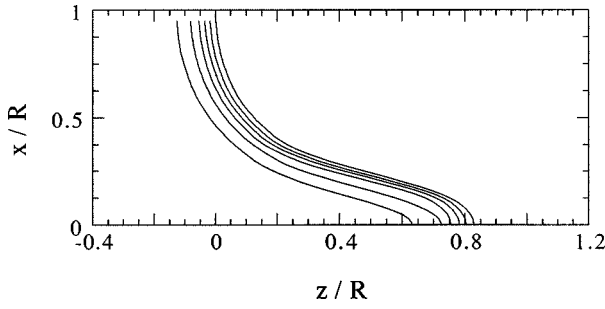


FIG. 2. The shape of a stationary curved flame with the expansion coefficient $\Theta=8$ observed in numerical simulations [9] in a tube of width $R=\lambda_c$ with ideally adiabatic and slip walls.

The general form of the coefficients C_1 , C_2 , and C_3 has been presented in [24]. On the other hand, the nonlinear terms of Eq. (79) remain the same independent of the Lewis number, viscosity, and the coefficient of thermal conduction.

IV. STATIONARY CURVED FLAMES

Let us consider dynamics and stability of 2D curved stationary flames propagating in tubes with ideally slip and adiabatic walls. An example of a curved stationary flame with $\Theta=8$ observed in 2D numerical simulations [6,9] for a tube of moderate width $R=\lambda_c$ is presented in Fig. 2. The configuration of a flame in a tube with ideal walls describes also the case of a flame front with a periodic spatial structure, since ideal walls may be treated as symmetry axes. In that case the tube width R determines half of the spatial period, which, consequently, equals 2 in the scaled units. Since we deal with the function ϕ related to the flame position f in a nonlinear way, Eq. (78), then in the following it is easier to consider periodic boundary conditions on ϕ , keeping in mind that these conditions are equivalent to adiabatic conditions at ideal walls placed in the points where $\partial f/\partial \eta=0$.

Dynamics of the stationary flames in the chosen configuration has been studied in [12] on the basis of the nonlinear equation (1). Stationary solution of Eq. (79) corresponds to a curved stationary flame front with $\phi=\phi(\eta)$, $W=U_w/U_f-1$, $A=0$, for which the complete time-dependent nonlinear equation (79) is reduced to the stationary equation (58). Solution of the stationary equation (58) has been found in [12] by the method of pole decomposition [15]

$$\phi_s = -\frac{\lambda_c}{2R} \frac{\Theta-1}{\pi\Theta(1+4\omega)} \sum_{\alpha=1}^{2M} \ln \sin\left(\pi \frac{\eta-\eta_\alpha}{2}\right), \quad (85)$$

where η_α are poles in the complex plane coming in conjugate pairs $\eta_\alpha, \eta_\alpha^*$ with imaginary parts $\text{Im } \eta_\alpha = -\text{Im } \eta_\alpha^*$. M is the total number of pole pairs and the designation

$$\omega = \frac{(\Theta-1)^3}{16\Theta^2} \quad (86)$$

is introduced for the value characterizing influence of flame generated vorticity on dynamics of the flame front [12]. The boundary conditions at the tube walls are taken into account by the periodic structure of the pole terms in the representa-

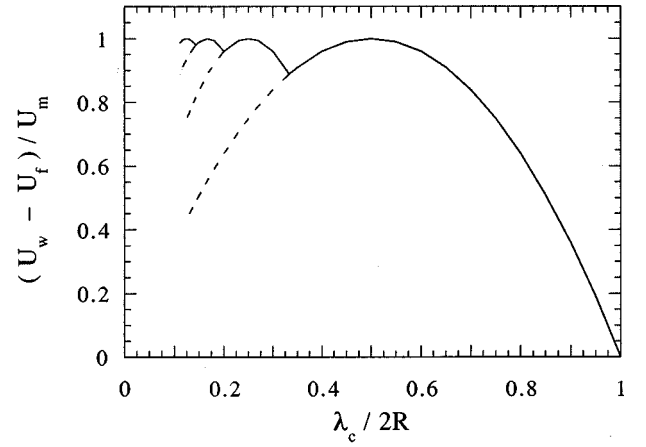


FIG. 3. Dependence of the scaled velocity amplification $(U_w - U_f)/U_m$ on the scaled inverse tube width $\lambda_c/2R$ for curved stationary flames. Solid line shows the solutions providing maximal flame velocity.

tion Eq. (85): $\ln \sin[(\pi/2)(\eta-\eta_\alpha)]$. For the solution with M pairs of poles the flame velocity is calculated from Eq. (58) as

$$U_w - U_f = 4U_m \frac{M\lambda_c}{2R} \left(1 - \frac{M\lambda_c}{2R}\right), \quad (87)$$

where the maximal velocity amplification is given by Eq. (3). Typical dependence of the velocity amplification on the scaled inverse tube width $\lambda_c/2R$ is shown in Fig. 3. One can find from Eq. (87) that for a fixed tube width R the maximal velocity of a curved stationary flame is provided by a solution with the number of pole pairs $M = \text{Int}[R/\lambda_c + \frac{1}{2}]$. The last result implies that for wide tubes solutions with a large number of poles become of importance: the wider the tube, the larger the number M of pole pairs.

The positions of the poles in the complex plane are determined by the set of equations

$$\begin{aligned} & \frac{\lambda_c}{2R} \frac{1+2\omega}{1+4\omega} \sum_{\alpha \neq \beta}^{2M-1} \left[1 + \text{sgn}(\text{Im } \eta_\alpha \text{Im } \eta_\beta) \frac{2\omega}{1+2\omega} \right] \\ & \times \cot\left(\pi \frac{\eta_\alpha - \eta_\beta}{2}\right) + i \text{sgn}(\text{Im } \eta_\alpha) \left[1 - \frac{4\omega M}{1+4\omega} \frac{\lambda_c}{2R} \right] = 0, \end{aligned} \quad (88)$$

that follows from Eq. (58) after substitution of the stationary solution Eq. (85). Particularly, in the simplest case of one pair of poles $M=1$ the pole positions may be chosen as $\eta_\alpha = i\beta, \eta_\alpha^* = -i\beta$ and the set of equations (88) is reduced to one equation for the parameter β ,

$$\frac{\lambda_c}{2R} \frac{1+2\omega}{1+4\omega} \left(1 - \frac{2\omega}{1+2\omega}\right) \cot(i\pi\beta) + i \left(1 - \frac{\lambda_c}{2R} \frac{4\omega}{1+4\omega}\right) = 0, \quad (89)$$

which defines the position of the pair of poles via the scaled tube width as

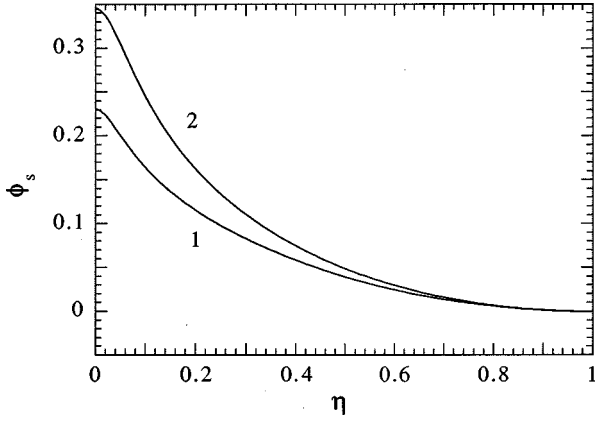


FIG. 4. Shapes of curved stationary flames with the expansion coefficient $\Theta=5$ for a tube width $R=2.16\lambda_c$. Solutions are described by two pairs of poles $M=2$ in the pole decomposition, curve 1 presents the principal solution, curve 2 shows the additional solution.

$$\cosh(\pi\beta) = \left\{ 1 - \frac{\lambda_c^2}{4R^2} \left(1 + 4\omega \left[1 - \frac{\lambda_c}{2R} \right] \right)^{-2} \right\}^{1/2}. \quad (90)$$

The pole positions depend also on the expansion coefficient of the flame front Θ , since parameter ω is a function of the expansion coefficient. It follows from Eq. (90) that a stationary curved flame is impossible in a narrow 2D tube of width $R < \lambda_c/2$, when the DL instability is suppressed by thermal conduction. In a tube of width $R > \lambda_c/2$ a stationary solution with one pair of poles develops as a result of the DL instability, while in the case of wider tubes solutions with a larger number of poles are possible. The bifurcations of the solution for the flame velocity Eq. (87) at the points $\lambda_c/2R = 1/3, 1/5, \dots$ that one can see in Fig. 3 correspond to transitions to solutions with a larger number of poles.

Therefore, for wide tubes $R > 3\lambda_c/2$ solution of Eq. (88) is not unique. Different solutions for a curved stationary flame front may have a different number of pole pairs M . Even more, for a fixed tube width and a fixed number of pole pairs M several stationary solutions are possible. For example, for a flame with the expansion coefficient $\Theta=5$ in the case of a tube width $R=2.16\lambda_c$ (i.e., for $\lambda_c/2R=0.231$) and two pairs of poles $M=2$ we have obtained two different solutions presented in Fig. 4. Flame fronts shown in Fig. 4 propagate downwards, so that the fresh fuel is below the front and the burnt matter is above the front. According to Eq. (87) both solutions have the same velocity of flame propagation, and,

as one can see in Fig. 4, they have similar shapes, though one solution is more curved than the other. It is interesting to compare the obtained solutions in the bifurcation point $\lambda_c/2R=1/3$ where the solutions with two pairs of poles $M=2$ intersect with the solution with one pair of poles $M=1$ determined by Eq. (90). At the bifurcation point $\lambda_c/2R=1/3$ the flame front presented by curve 1 in Fig. 4 coincides in shape with the solution with one pair of poles $M=1$, which is the dominant solution for narrow tubes with $\lambda_c/2R > 1/3$. By this reasoning the solution presented by curve 1 is likely to happen in reality (at least close to the bifurcation point), in spite of the fact that the other solution is more curved. In the following we will call the solution shown by curve 1 in Fig. 4 “the principal solution,” while the solution shown by curve 2 will be called “the additional solution.”

V. STABILITY ANALYSIS: THE LINEARIZED EQUATION AND THE EIGENVALUE PROBLEM

In order to study stability of the stationary solutions described in the preceding section, we consider evolution of perturbations of an infinitesimal amplitude. Since the unperturbed solution is stationary, then the perturbations take the form

$$\tilde{\phi}(\eta, \tau) = \tilde{\phi}(\eta) \exp(S\tau), \quad (91)$$

where S is the scaled instability growth rate. Development of perturbations is described by Eq. (79) linearized around the stationary solution ϕ_s ,

$$\frac{\partial^2}{\partial \eta^2} \tilde{\Psi}_0 - \tilde{\Psi}_1 = 0, \quad (92)$$

where

$$\begin{aligned} \tilde{\Psi}_0 = & \frac{\Theta+1}{2\Theta} S^2 \hat{\Phi}^{-1} \tilde{\phi} + \left(1 + \varepsilon \frac{\Theta \ln \Theta}{\Theta-1} \hat{\Phi} \right) S \tilde{\phi} + \Theta \frac{\partial \phi_s}{\partial \eta} \frac{\partial \tilde{\phi}}{\partial \eta} \\ & + \frac{(\Theta-1)^3}{8\Theta} \left[\frac{\partial \phi_s}{\partial \eta} \frac{\partial \tilde{\phi}}{\partial \eta} - \hat{\Phi} \phi_s \hat{\Phi} \tilde{\phi} \right] \\ & - \frac{\Theta-1}{2} \left(\hat{\Phi} \tilde{\phi} + \frac{\lambda_c}{2\pi R} \frac{\partial^2 \tilde{\phi}}{\partial \eta^2} \right), \end{aligned} \quad (93)$$

and

$$\begin{aligned} \tilde{\Psi}_1 = & -\frac{\Theta+1}{2} \frac{\partial^2}{\partial \eta^2} \left(\frac{\partial \phi_s}{\partial \eta} \frac{\partial \tilde{A}}{\partial \eta} \right) + S^2 (\Theta-1)^2 \frac{\Theta+1}{8\Theta^2} \left[\hat{\Phi} \phi_s \hat{\Phi} \tilde{\phi} - \frac{\partial \phi_s}{\partial \eta} \frac{\partial \tilde{\phi}}{\partial \eta} \right] + \frac{\Theta-1}{2\Theta} S \left[S \frac{\partial \tilde{\phi}}{\partial \eta} \frac{\partial \phi_s}{\partial \eta} + \hat{\Phi} \phi_s \frac{\partial^2}{\partial \eta^2} \left(\frac{\Theta-1}{2} \tilde{\phi} - \tilde{A} \right) \right. \\ & \left. + \frac{\Theta-1}{2} \hat{\Phi} \tilde{\phi} \frac{\partial^2 \phi_s}{\partial \eta^2} \right] + S^2 \left(\phi_s \frac{\partial^2 \tilde{\phi}}{\partial \eta^2} \right) + \frac{(\Theta-1)^2}{4\Theta^2} S \left[\frac{\partial \phi_s}{\partial \eta} \frac{\partial}{\partial \eta} (S \tilde{\phi} + \hat{\Phi} \tilde{\phi}) + \left(\frac{\partial \tilde{\phi}}{\partial \eta} + 2 \frac{\partial \tilde{A}}{\partial \eta} \right) \hat{\Phi} \frac{\partial \phi_s}{\partial \eta} \right] \\ & + S \hat{\Phi} \left[\frac{(\Theta-1)^2}{2\Theta} \hat{\Phi} \phi_s \hat{\Phi} \tilde{\phi} + S \phi_s \hat{\Phi} \tilde{\phi} - \frac{\Theta-1}{2\Theta} \frac{\partial \phi_s}{\partial \eta} \frac{\partial \tilde{A}}{\partial \eta} \right]. \end{aligned} \quad (94)$$

Here one has for the perturbed value A

$$\tilde{A} = \frac{\Theta + 1}{2\Theta} \hat{\Phi}^{-1} S \tilde{\phi}. \quad (95)$$

With the periodic boundary conditions imposed on the perturbations $\tilde{\phi}$ the linearized equation (92) poses an eigenvalue problem with the instability growth rate S being the eigenvalue and the perturbation $\tilde{\phi}$ being the eigenfunction.

The eigenvalue problem has been solved numerically. Due to the periodic boundary conditions any perturbation $\tilde{\phi}$ may be presented in the form

$$\tilde{\phi} = \sum_m^{M_p} \tilde{\phi}_m \cos(m\pi\eta). \quad (96)$$

The unperturbed stationary solution was approximated by a similar superposition of Fourier harmonics

$$\phi_s = \sum_m^{M_s} \phi_m \cos(m\pi\eta), \quad (97)$$

where the number of harmonics employed to describe the perturbations M_p and the stationary solution M_s has been determined by accuracy requirements. We kept the accuracy in the expansion of the stationary solution about 1%, while the resulting accuracy of the eigenvalue problem was about 5%. For the tube widths $3\lambda_c/2 < R < 5\lambda_c/2$ (i.e., for $1/5 < \lambda_c/2R < 1/3$) the number of harmonics needed to achieve such accuracy in the numerical solution has been up to 20.

Substituting the Fourier representations Eqs. (96),(97) into the linearized equation (92) and comparing the coefficients in front of the respective cosine functions $\cos(m\pi\eta)$, $m=0,1,2,\dots,M_p$, we obtain a system of algebraic equations for the unknown amplitudes $\tilde{\phi}_m$ that determine the eigenvector of the problem. Zero determinant of the obtained system provides us with the dispersion relation for the instability growth rate. The instability growth rate S is given by the roots of the determinant, which were calculated by a modified one-dimensional Newton method in the rectangular region of the complex plane ("the carpet method").

VI. RESULTS AND DISCUSSION

We have investigated stability of the stationary solutions ϕ_s of the nonlinear equation (79) corresponding to curved stationary flames in ideal tubes in a wide range of tube widths $\lambda_c/2 < R < 5\lambda_c/2$ (i.e., for $1/5 < \lambda_c/2R < 1$) for flames with different expansion coefficients $\Theta=3-10$ typical for laboratory flames.

For rather narrow tubes with $1/3 < \lambda_c/2R < 1$ curved stationary flames are represented by the solution with one pair of poles $M=1$ with the pole positions determined by the tube width and the flame expansion coefficient through Eq. (90). We have found that in this range of the tube widths the instability growth rate is negative $S < 0$ and the curved stationary flames are stable. This result agrees well with the results of numerical simulations of flame dynamics in ideally slip and adiabatic tubes performed on the basis of the com-

plete set of hydrodynamical equations including thermal conduction, fuel diffusion, viscosity, and chemical kinetics [6].

We found that in wider tubes $1/5 < \lambda_c/2R < 1/3$ the solution with one pair of poles, $M=1$, becomes unstable and the curved flame front is now determined by the solutions with two pairs of poles $M=2$. First of all the analysis was concentrated on the principal solution with two pairs of poles shown in Fig. 4 by curve 1, since this solution goes over continuously into the solution with $M=1$ in the bifurcation point $\lambda_c/2R=1/3$. The instability growth rate for the principal solution is shown in Fig. 5 by curve 1 for a flame with the expansion coefficient $\Theta=5$ versus the scaled inverse tube width. As is shown in Fig. 5, close to the bifurcation point the principal solution is stable, but increase of the tube width makes the stationary solution less stable. The growth rate goes over to the positive half plane at $\lambda_c/2R=0.231$ and the stationary curved flame described by the principal solution becomes unstable ($\text{Re } S > 0$) for the tube width larger than the critical value $R > R_w = 2.16\lambda_c$ (i.e., for $\lambda_c/2R < 0.231$). The perturbation function $\tilde{\phi}$ at the stability limit $R=R_w$ for a flame with the expansion coefficient $\Theta=5$ is presented in Fig. 6. The respective perturbation of the flame front position \tilde{f} at the stability limits coincides with the perturbed function $\tilde{\phi}$ with the accuracy of the nonlinear equation (79). As one can see, the perturbation function is rather smooth without well pronounced wrinkles and, in that sense, it resembles the unperturbed stationary solution shown in Fig. 4. Still one can hardly distinguish the hump and the cusp for the perturbation function taking into account that in the linear stability problem the sign of the perturbation amplitude is indefinite.

Curved flames with other expansion coefficients $\Theta=3-10$ have similar stability properties. In narrow tubes $1/3 < \lambda_c/2R < 1$ the stationary flame front determined by the solution with one pair of poles $M=1$ is stable. For wider tubes $1/5 < \lambda_c/2R < 1/3$ the shape of a stationary curved flame is given by the principal solution with two pairs of poles $M=2$, but this solution becomes unstable for a sufficiently wide tube. The critical tube width for which the prin-

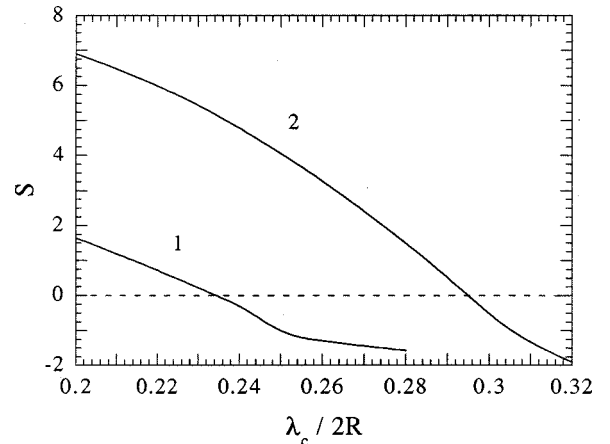


FIG. 5. The scaled instability growth rate vs the scaled inverse tube width for flames with the expansion coefficient $\Theta=5$. Curve 1 shows stability of the principal solution, curve 2 shows stability of the additional solution.

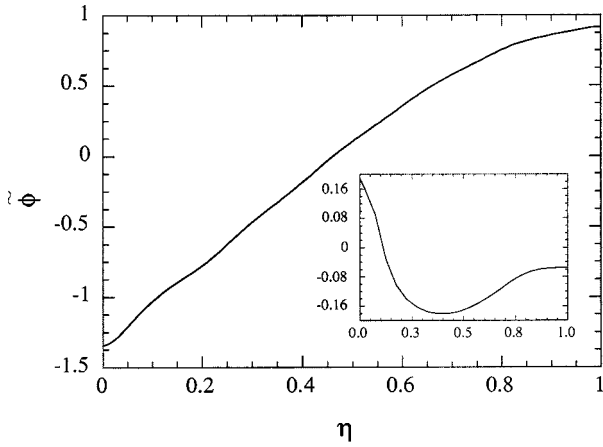


FIG. 6. The perturbation function $\tilde{\phi}$ at the stability limit $R = 2.16\lambda_c$ of the principal stationary solution. The expansion coefficient of the flame is $\Theta = 5$. The inset presents possible flame shape resulting from the instability at the nonlinear stage.

principal solution loses stability is shown in Fig. 7 versus the expansion coefficient of the flame. The critical value of the parameter $\lambda_c/2R_w$ corresponding to the stability limits decreases with the decrease of the expansion coefficient, which implies that the smaller the expansion coefficient, the larger the stability domain of curved stationary flames. Taking into account that for very small expansion coefficients $\Theta - 1 \ll 1$ curved stationary flames are stable independent of the tube width [15] we can expect that the critical tube width goes to infinity, $R_w \rightarrow \infty$, with $\Theta \rightarrow 1$ and the respective critical value of the parameter $\lambda_c/2R_w$ goes to zero, $\lambda_c/2R_w \rightarrow 0$, as the expansion coefficient approaches unity, $\Theta \rightarrow 1$. However numerical solution in these regions is very time consuming, so that we checked this tendency only for Θ in the range from $\Theta = 10$ to $\Theta = 3$, which corresponds to laboratory flames with realistic expansion coefficients.

It is interesting to note that for all investigated tube widths and flame expansion coefficients the perturbation growth rate

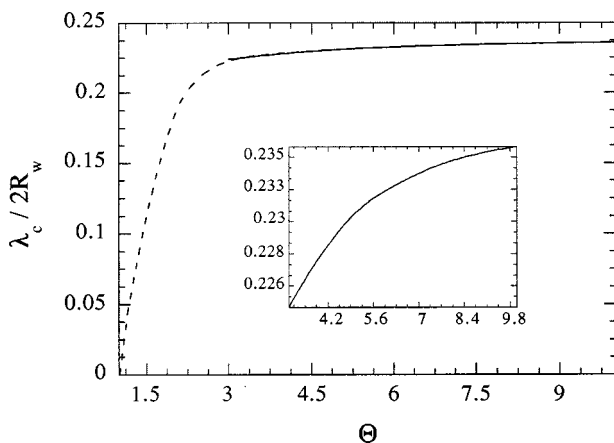


FIG. 7. The stability limits of the principal solution for a curved stationary flame vs the expansion coefficient of the flame front. The dashed line shows extrapolation of the present results into the domain of small expansion coefficients by use of [15]. The inset shows the obtained dependence for realistic expansion coefficients $\Theta = 3-10$.

is a real value with zero imaginary part. The last fact implies that at the stability limits, for which $\text{Re } S = 0$, the more general condition, $S = 0$, holds and the linearized equation (92) takes a simple form

$$\Theta \frac{\partial \phi_s}{\partial \eta} \frac{\partial \tilde{\phi}}{\partial \eta} + \frac{(\Theta - 1)^3}{8\Theta} \left[\frac{\partial \phi_s}{\partial \eta} \frac{\partial \tilde{\phi}}{\partial \eta} - \hat{\Phi} \phi_s \hat{\Phi} \tilde{\phi} \right] - \frac{\Theta - 1}{2} \left(\hat{\Phi} \tilde{\phi} + \frac{\lambda_c}{2\pi R_w} \frac{\partial^2 \tilde{\phi}}{\partial \eta^2} \right) = 0. \quad (98)$$

Equation (98) is nothing but the scaled linearized stationary equation (1) written in the considered 2D configuration. Therefore the problem of stability limits of a curved stationary flame can be solved even in the scope of the stationary equation (1) for curved flames, while the complicated time-dependent nonlinear terms of the complete equation (79) do not influence the stability limits. The problem of stability limits is formulated as an eigenvalue problem of the stationary nonlinear equation (1) linearized around the stationary solution with the inverse critical tube width $\lambda_c/2R_w$ playing the role of an eigenvalue and perturbation of the flame front playing the role of the eigenfunction.

The important question is the outcome of the obtained instability at the nonlinear stage: at this point interpretation of the instability is not obvious at all. As one can see in Fig. 6, perturbations of the flame front that grow due to the instability are rather smooth and resemble the shape of the stationary curved flames. Because of the smooth shape of the perturbation function it is unlikely that the instability leads to strong wrinkling of a flame front as described in [8]. For this reason the first guess about the outcome of the instability is that development of the instability makes a flame front more curved, though it preserves the smooth flame shape. One might expect that the principal stationary solution shown by curve 1 in Fig. 4 (less curved solution) develops because of the instability into the additional stationary solution shown by curve 2 (more curved solution). In order to check this possibility, we have investigated stability of the additional solution as well. The instability growth rate for the additional solution is presented in Fig. 5 by curve 2 for a flame with the expansion coefficient $\Theta = 5$. In this case the additional solution becomes unstable for narrower tubes than the principal one with the critical tube width for the additional solution being $R = 1.69\lambda_c$ (i.e., $\lambda_c/2R = 0.295$). Therefore the principal solution cannot develop into the additional one: when the principal solution just loses stability, the additional solution is already strongly unstable. At the same time we have not found any other stable stationary solution of the same period for the tube width under consideration. Thus the first guess that the principal solution goes over to another stationary solution of a similar smooth shape is not confirmed.

The other guess is that the instability starts from smooth perturbations at the linear stage, but leads to an extra cusp at a flame front at the nonlinear stage of the instability similar to Fig. 1. This guess is illustrated in the inset of Fig. 6, where the perturbation function $\tilde{\phi}$ multiplied by a small factor 0.08 is formally added to the principal stationary solution. The flame front in the inset propagates downwards. As one can see, the resulting flame shape looks like the flame shape in

Fig. 1(b), which is an intermediate step in the development of the secondary DL instability. It is noteworthy that the starting flame shape in Fig. 1(a) resembles the stationary flames described by the method of pole decomposition, while the final flame shape in Fig. 1(c) is quite different from the shapes found by this method. Besides, the velocity of flame propagation in Fig. 1(c) noticeably exceeds the maximal velocity of curved stationary flames obtained by the method of pole decomposition. A strong point in favor of the second assumption on the nonlinear outcome of the obtained instability is that the stability limits found in the present paper are quite close to the stability limits evaluated for the secondary DL instability in [8,9]. Particularly, the curved flames with an extra cusp like that presented in Fig. 1 have been observed in the 2D numerical simulations [9] for the tube width $R = 2\lambda_c$ (i.e., for the scaled parameter $\lambda_c/2R = 0.25$) and for the expansion coefficient of the flame $\Theta = 6.5$. According to the results of the present paper, the stationary curved flame front with the expansion coefficient $\Theta = 6.5$ loses stability for the critical tube width $R_w = 2.14\lambda_c$ (the scaled inverse tube width is $\lambda_c/2R = 0.234$). Taking into account the accuracy of the present paper and the accuracy of the numerical simulations [9], one can say that the obtained stability limits agree very well with the tube width for which the secondary DL instability has been observed in [9]. Besides, the numerical experiments [9] have been performed for nonzero Mach numbers of the fuel flow determined as the ratio of the flame velocity to the sound speed in the fuel, while in the present paper isobaric flames are considered. Particularly, curved flames with an extra cusp presented in Fig. 1 have been observed for the Mach number equal to 0.1. Since increase of the Mach number of the fuel flow enhances the DL instability, it is expected that for isobaric flames the curved flames with extra cusps develop in somewhat wider tubes (about 10% wider), which comes even closer to the stability limits found in the present paper. The numerical simulations [9] have been performed on the basis of the complete set of hydrodynamical equations including thermal conduction, fuel diffusion, viscosity, and chemical kinetics. Dynamics of a flame in a 2D tube with ideally adiabatic and slip walls has been investigated.

It should be pointed out that the semiquantitative estimates of the stability limits of the secondary DL instability performed in [8] are also rather close to the stability limits obtained in the present paper. For example, for the flames with the expansion coefficient $\Theta = 8.3$ the critical tube width was evaluated in [8] as $R_w \approx 2.5\lambda_c$, while calculations of the present paper provide a close value, $R_w \approx 2.35\lambda_c$. Besides, the estimates [8] have been performed under the assumption of a well developed secondary DL instability far from the stability limits and one should not expect more than an order of magnitude evaluation on the basis of the analysis [8].

It is interesting to compare the theoretical results of the present paper with the experimental results on the DL instability of flames in tubes and of expanding flames [26–28,32,29,30]. At this point one should notice that experiments on flames in tubes have been performed typically in the configuration of cylindrical tubes and characteristic Reynolds numbers have been calculated with respect to the tube diameter. In this sense the width of an ideal 2D channel considered in the present paper should be treated as a tube

radius because of the symmetry reasons. Then the linear theory [4] predicts development of the primary DL instability for the Reynolds numbers $Re > 20$ in the case of a flame with unit Lewis number and constant transport coefficients. In the case of flames with a realistic dependence of thermal conduction coefficient on temperature $\kappa \propto \sqrt{T}$ the critical Reynolds number for the primary DL instability becomes somewhat larger. For example, in the case of propane flames the primary instability of flames in tubes is expected at $Re = 30\text{--}40$ [24]. However, the primary DL instability is rather difficult for observations in tubes since it results in smooth stationary flame shapes. As has been pointed out in [8], such stationary curved flames are observed for flames in tubes with Reynolds numbers up to a few hundred (see also [26–28,32]). On the contrary, the secondary DL instability is clearly seen on flame fronts in tubes in the form of fine cellular structure or flame self-turbulization. The secondary DL instability is well developed in tubes at $Re \approx 10^3$ [8]. Results of the present paper give the stability limits of the secondary DL instability $Re \approx 80$ and $Re \approx 140\text{--}160$ for flames with constant transport coefficients and for propane flames, respectively. Besides, one should remember that the secondary instability becomes clearly visible only for flames sufficiently far from the stability limits. For example, the qualitative estimates [8] predict the stability limits of the secondary instability about $Re = 100\text{--}200$ and indicated that the instability may be clearly observed only at $Re \approx 10^3$. At lower Reynolds numbers flame stretch slows down the secondary instability considerably. Taking into account the estimates [8] the results of the present paper agree with the experimental observations of the secondary DL instability of flames in tubes. In a number of experiments detonation triggering by a turbulent flame has been reported (see, for example, [1,2]). Triggering of the detonation ahead of the flame propagating in a closed tube due to the weak shocks and sound waves generated by the accelerated flames has been considered in [31]. In the scope of the present analysis it is impossible to draw any conclusion about transition to a detonation, since the analysis has been performed using the isobaric approximation.

The secondary DL instability has been observed also in experiments on expanding flames, for which both the primary and secondary instability may be clearly seen on a flame front. Particularly, it was observed in [30] that flame surface in lean methane-air mixtures becomes wrinkled at some critical radius of the front with characteristic cell size about 2 cm. As the flame radius increased together with the cell size, a fine structure developed at the initial flame cells. The size of the primary cells at this instant was about 6–10 cm. While the small cells at the flame front may be interpreted as the primary DL instability, development of the fine structure on larger cells corresponds to the secondary instability. It is remarkable that the secondary instability starts, when the cell size increases with respect to the initial one by a factor of 3–5. Particularly, according to the present theoretical results the expected increase of the cell size is about 4, which agrees very well with the experimental observations. Similar dynamics of cells at the front of an expanding flame has been observed in [29].

Thus, good agreement of the stability limits for curved stationary flames obtained in the present paper with the

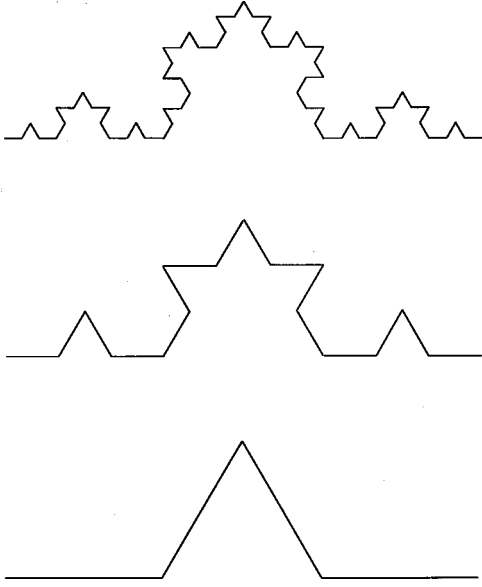


FIG. 8. Three steps in construction of the Koch curve.

evaluations of the stability limits in the numerical simulations [9], in the semiquantitative analysis [8], and with experimental observations supports the assumption that the instability found in the present paper is the secondary DL instability discussed in the Introduction. Still, the conclusion about the obtained instability is possible only on the basis of direct numerical simulations of the nonlinear time-dependent equation (79) that we plan to publish in the future.

As has been pointed out, development of the secondary DL instability far from the stability limits may be interpreted as self-turbulization of a flame front [10]. Therefore, it is interesting to evaluate the fractal dimension of a turbulized flame front on the basis of the present theoretical results. The fractal structure of a flame front may be described as cascading humps and cusps: humps of smaller scales develop on humps of large scales and so on. The general idea of the process may be understood from the Koch curves constructed as a cascade of triangles as shown in Fig. 8 [25]. Taking into account similarity of a fractal flame and the Koch curve we can estimate increase of the flame velocity for a spontaneously turbulized flame [10,11]. Let every step of the fractal cascade decrease the cell size by a factor $b: \lambda_{k+1} = \lambda_k/b$, and increase the flame velocity by a factor $\beta, U_{k+1} = \beta U_k$. The cascading process is limited from below by the cutoff wavelength λ_c and limited from above by the tube width R . The fractal structure implies a large number of cascades $N = \ln(R/\lambda_c)/\ln b \gg 1$ and the fractal flame velocity is

$$U_{\text{fractal}} = U_N = U_f \beta^N = U_f \left(\frac{R}{\lambda_c} \right)^d, \quad (99)$$

where $d = \ln \beta / \ln b$ is the excess of the fractal dimension over the embedding dimension. The fractal excess is typically different in 2D and 3D configurations and the fractal dimension

of the self-turbulized flame front is given by the values $1 + d_{2D}$ and $2 + d_{3D}$ for 2D and 3D flames, respectively. The fractal dimension (or the fractal excess d) of a flame front is the main parameter that determines velocity of a spontaneously turbulized flame on large length scales much larger than the cutoff wavelength. One can estimate the fractal excess on the basis of the theory of dynamics and stability of curved stationary flames considering a curved stationary flame as one step of the cascade similar to the Koch triangles. Then increase of the flame velocity on one step of the cascade (the factor β) is evaluated by the maximal amplification of the flame velocity for a curved stationary flame $\beta = 1 + U_m/U_f$. In the 2D geometry the maximal velocity amplification is given by the analytical formula Eq. (3), so that the factor β in the 2D case depends on the expansion coefficient of the flame as

$$\beta_{2D} = 1 + \frac{\Theta}{2} \frac{(\Theta - 1)^2}{\Theta^3 + \Theta^2 + 3\Theta - 1}. \quad (100)$$

In the 3D case the respective velocity amplification is approximately twice larger and the factor β may be estimated as $\beta_{3D} = 1 + 2(\beta_{2D} - 1)$ [13]. For the realistic expansion coefficients $\Theta = 5-10$ the factor β is about $\beta_{2D} = 1.25-1.35$ and $\beta_{3D} = 1.5-1.7$ for 2D and 3D geometries, respectively. The increase of the length scale for one step of the fractal structure (the factor b) is given by the stability limits of curved stationary flames $b = R_w/R_c$. Here R_c is the tube width at which the DL instability overcomes the stabilizing influence of thermal conduction and curved stationary flames develop, while R_w is the tube width for which curved stationary flames become unstable with respect to the secondary DL instability. In the 2D configuration of a tube with ideally slip and adiabatic walls one has $R_c = \lambda_c/2$. The stability limits of curved stationary flames obtained in the present paper, the evaluations [8], and the numerical simulations [9] give the estimate $b = R_w/R_c = 4-5$ for flames with realistic expansion coefficients. Taking these values into account we can evaluate the fractal excess for spontaneously turbulized flames in 2D and 3D geometries as

$$d_{2D} = 0.16-0.19, \quad d_{3D} = 0.3-0.35 \quad (101)$$

and the respective fractal dimensions as 1.16-1.19 and 2.3-2.35. The analytical estimates agree quite well with the experimental results on the fractal dimension of accelerating self-turbulized spherical flames, where the fractal dimension 2.33 has been obtained for expanding 3D flames [10].

ACKNOWLEDGMENTS

This work was supported in part by the Swedish National Board for Industrial and Technical Development, by the Swedish Natural Science Research Council, and by the Swedish Royal Academy of Sciences.

- [1] Ya. B. Zeldovich, G. I. Barenblatt, V. B. Librovich, and G. M. Makhviladze, *The Mathematical Theory of Combustion and Explosion* (Consultants Bureau, New York, 1985).
- [2] F. A. Williams, *Combustion Theory* (Benjamin, Reading, MA, 1985).
- [3] L. D. Landau and E. M. Lifshitz, *Fluid Mechanics* (Pergamon, Oxford, 1987).
- [4] P. Pelce and P. Clavin, *J. Fluid Mech.* **124**, 219 (1982).
- [5] B. Denet and P. Haldenwang, *Combust. Sci. Technol.* **104**, 143 (1995).
- [6] V. V. Bychkov, S. M. Golberg, M. A. Liberman, and L. E. Eriksson, *Phys. Rev. E* **54**, 3713 (1996).
- [7] V. V. Bychkov, A. I. Kleev, M. A. Liberman, and S. M. Golberg, *Phys. Rev. E* **56**, R36 (1997).
- [8] Ya. B. Zeldovich, A. G. Istratov, N. I. Kidin, and V. B. Librovich, *Combust. Sci. Technol.* **24**, 1 (1980).
- [9] O. Yu. Travnikov, V. V. Bychkov, and M. A. Liberman, *Phys. Fluids* (to be published).
- [10] Y. I. Gostintsev, A. G. Istratov, and Y. V. Shulenin, *Combust., Explos. Shock Waves* **24**, 70 (1988).
- [11] V. V. Bychkov and M. A. Liberman, *Phys. Rev. Lett.* **76**, 2814 (1996).
- [12] V. V. Bychkov, *Phys. Fluids* **10**, 2091 (1998).
- [13] V. V. Bychkov and A. I. Kleev, *Phys. Fluids* **11**, 1890 (1999).
- [14] G. I. Sivashinsky, *Acta Astron.* **4**, 1177 (1977).
- [15] O. Thual, U. Frish, and M. Henon, *J. Phys. (France)* **46**, 1485 (1985).
- [16] G. Joulin, *J. Phys. (France)* **50**, 1069 (1989).
- [17] S. Gutman and G. I. Sivashinsky, *Physica D* **43**, 129 (1990).
- [18] L. Filyand, G. I. Sivashinsky, and M. L. Frankel, *Physica D* **72**, 110 (1994).
- [19] S. I. Blinnikov and P. V. Sasorov, *Phys. Rev. E* **53**, 4827 (1996).
- [20] Z. Olami, B. Galanti, O. Kupervasser, and I. Procaccia, *Phys. Rev. E* **55**, 2649 (1997).
- [21] B. Galanti, O. Kupervasser, Z. Olami, and I. Procaccia, *Phys. Rev. Lett.* **80**, 2477 (1998).
- [22] M. L. Frankel and G. I. Sivashinsky, *Combust. Sci. Technol.* **29**, 207 (1982).
- [23] M. Matalon and B. J. Matkowsky, *J. Fluid Mech.* **124**, 239 (1982).
- [24] G. Searby and D. Rochwerger, *J. Fluid Mech.* **231**, 529 (1991).
- [25] B. B. Mandelbrot, *The Fractal Geometry of Nature* (Freeman, San Francisco, 1983).
- [26] H. Tsien, *J. Appl. Mech.* **18**, 188 (1951).
- [27] M. Uberoi, *Phys. Fluids* **2**, 72 (1959).
- [28] T. Maxworthy, *Phys. Fluids* **5**, 407 (1962).
- [29] L. A. Gussak, E. N. Sprintsina, and K. I. Shelkin, *Fiz. Goreniya Vzryva* **4**, 358 (1968).
- [30] P. Ivashchenko and V. Rumiantsev, *Fiz. Goreniya Vzryva* **2**, 83 (1966).
- [31] M. A. Liberman, V. V. Bychkov, S. M. Golberg, and L. E. Eriksson, *Combust. Sci. Technol.* **136**, 221 (1998).
- [32] G. H. Markstein, *Nonsteady Flame Propagation* (Pergamon, Oxford, 1964).